Regular Article

# Targeted delivery and pH-responsive release of doxorubicin to cancer cells using calcium carbonate/hyaluronate/glutamate mesoporous hollow spheres

Yuming Guo [a,b,*], Han Li [a], Weike Shi [a], Jie Zhang [a], Jing Feng [a], Xiaoli Yang [a], Kui Wang [a], Hua Zhang [a], Lin Yang [a,b,*]

[a] Collaborative Innovation Center of Henan Province for Green Manufacturing of Fine Chemicals, Key Laboratory of Green Chemical Media and Reactions, Ministry of Education, Henan Normal University, Xinxiang, Henan 453007, PR China
[b] Henan Key Laboratory of Green Chemical Media and Reactions, School of Chemistry and Chemical Engineering, Henan Normal University, Xinxiang, Henan 453007, PR China

## GRAPHICAL ABSTRACT

Herein, calcium carbonate/hyaluronate/glutamate mesoporous hollow spheres were prepared and used for targeted delivery and pH-sensitive release of anticancer drugs to treat human cancers.
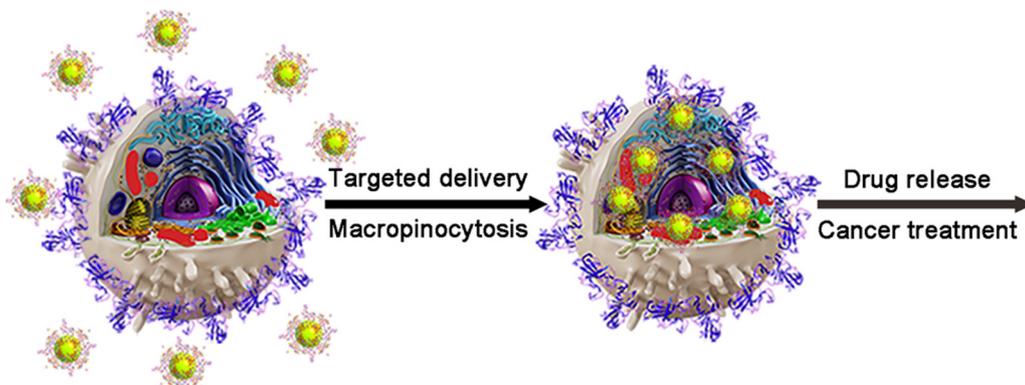
## ABSTRACT

Currently, the efficacies of the existing anticancer drugs used in chemotherapy are still unsatisfactory. Therefore, drug delivery system has received considerable research interest. In the present study, calcium carbonate/hyaluronate/glutamate mesoporous hollow spheres are prepared through a facile method. The results indicate that the mesoporous hollow spheres can efficiently load the anticancer drug doxorubicin. Through the specific binding of hyaluronate on hollow spheres with CD44 receptors overexpressed on cancer cells, the drug-loaded hollow spheres can be specifically delivered to target cancer cells. Owing to the gradually dissolution of calcium carbonate in the weak acidic microenvironment of cancer cells, the loaded doxorubicin can be released over the period of 14 days with pH-responsive and sustained manner to specifically and significantly treat cancers. Through loaded onto the hollow spheres, the $IC_{50}$ value of doxorubicin for HeLa cancer cells is 0.0113 μg/mL, much lower than that of the free doxorubicin (0.0801 μg/mL). However, the $IC_{50}$ value of doxorubicin for V79-4 cells is 0.2032 μg/mL, obviously

---

* Corresponding authors at: Henan Key Laboratory of Green Chemical Media and Reactions, School of Chemistry and Chemical Engineering, Henan Normal University, Xinxiang, Henan 453007, PR China.
   *E-mail addresses:* guoyuming@htu.edu.cn (Y. Guo), yanglin1819@163.com (L. Yang).

higher than that of the free DOX (0.1396 µg/mL). The specificity of the doxorubicin between normal and cancer cells can be enhanced about 10-fold. The current study suggests the possible application of pH-responsive inorganic carriers for efficiently treatment of human cancers.

# 1. Introduction

Currently, on account of the unfavorable pharmacokinetics, poor biodistribution and selectivity, the treatment efficacies of the existing chemotherapeutic drugs still do not meet the clinical demands [1–4]. Because of the significant enhancement of treatment efficacy and reduction of the systemic side effects of the free drugs by altering the pharmacokinetics and biodistribution, drug delivery system (DDS) has attracted considerable research interest [5–8]. Practically, an ideal DDS should eliminate the tissue damage on accidental extravasation, protect the drugs from premature degradation, reduce the side effects on nontarget tissues, and increase the local concentrations of the drugs [9]. In addition, the facile preparation and formulation, high drug loading capacity, and specific delivery to target cancer cells are critical for their clinical application [10,11]. Moreover, it is also important to release the drug in response to stimuli associated with the specific microenvironmental changes of cancer cells with sustained manner [12,13]. Previously, many studied DDS are constructed using polymers [14,15], lipids [16], and surfactants [17]. Recently, inorganic materials were considered as promising DDS candidates because of the simple preparation and reduced involvement of toxic agents, such as mesoporous silica [18–20], iron oxide [21], and hydroxide [22]. Similar to these inorganic drug carriers, $CaCO_3$ also might be an ideal DDS candidate because of the good biocompatibility and biodegradability [23–25].

Herein, $CaCO_3$/hyaluronate/glutamate hybrid mesoporous hollow spheres ($CaCO_3$/HA/Glu MHSs) were prepared through a facile strategy under mild conditions. The results indicate the simultaneous presence of two types of mesopores in MHSs. This interesting property contributes to the efficient loading and sustained release of anticancer drug doxorubicin (DOX). Furthermore, because of the inherently good biocompatibility, pH sensitivity, and biodegradability of $CaCO_3$, $CaCO_3$/HA/Glu MHSs can release the DOX in controlled and sustained manner in response to the weak acidic microenvironment of cancer cells. More importantly, because of the highly specific binding of HA with CD44 receptor overexpressed on cancer cells [26,27], $CaCO_3$/HA/Glu/DOX could be specifically delivered to target cancer cells. Using $CaCO_3$/HA/Glu MHSs as drug carrier, the specificity of DOX between normal cells and cancer cells is enhanced about 10-fold. The specificity of the DOX and the total drug release period are both much better than our previous results [28,29]. Together with our previous studies [23,25,28–30], the present study further demonstrates and expands the applications of pH-responsive inorganic materials as drug carriers to efficiently treat cancers.

# 2. Experimental

## 2.1. Chemicals

Calcium chloride ($CaCl_2$, ACS grade), sodium carbonate ($Na_2CO_3$, ACS grade), sodium hyaluronate (BioReagent grade), sodium bicarbonate (ACS grade), DOX (98%), sodium glutamate (BioReagent grade), and 3-(4,5-dimethylthiazol-2-yl)-2,5,diphenyl tetrazolium bromide (MTT, BioReagent grade) were purchased from Sigma-Aldrich CO. Eagle's minimum essential medium (EMEM), fetal bovine serum (FBS), and antibiotic-antimycotic solution (100 X) were purchased from Thermo Fisher Scientific Inc. All chemicals were used as received without further purification.

## 2.2. Preparation of CaCO₃/HA/Glu MHSs

The $CaCO_3$/HA/Glu MHSs were prepared as follows. Briefly, $CaCl_2$ aqueous solution (10.0 mL, 5 mM) was added slowly dropwise into 30 mL of mixed aqueous solution of Glu (5 mM) and HA (0.05 g) and moderate stirred for 2 h at 25 °C. Then, the aqueous solution of $Na_2CO_3$ (5 mM, 10 mL) was added and reacted for 24 h at 25 °C. Finally, the product was collected by centrifugation and rinsed with DD water and absolute ethanol for several times. The as-prepared product was dried under vacuum and denoted as $CaCO_3$/HA/Glu MHSs. For comparison, the experiments were also performed in the sole presence of HA or Glu or in the absence of HA and Glu under nearly identical conditions as the typical experiment.

## 2.3. Characterization

In the current study, the size and morphology of the samples were determined by scanning electron microscopy (SEM, JSM-6390LV, JEOL) and high-resolution transmission electron microscopy (HR-TEM, JEM-2100, JEOL). The crystal phases of the samples were determined by powder X-ray diffraction (XRD) using a D8ADVANCE X-ray diffractometer (Bruker axs Com., Germany) with graphite monochromatized Cu Kα radiation ($\lambda$ = 0.15406 nm). The XRD patterns of the samples were recorded in the 2θ range of 20-70°. The organic contents of the samples were determined by thermogravimetry-differential scanning calorimetry (TG-DSC, STA 449C, NETZSCH) analysis in the range of 25-900 °C with a linear heating rate of 10 °C/min. The specific surface area and pore size distribution were analyzed through the Brunauer–Emmett–Teller (BET) determination at liquid nitrogen temperature using $N_2$ as an adsorbent (Gemini 2380, Micromeritics).

## 2.4. DOX loading and the incorporation efficiency

$CaCO_3$/HA/Glu MHSs (7 mg) were mixed with DOX aqueous solution (7 mL, 100 µg/mL) and shaken in an orbital shaker for 24 h at 25 °C to load the DOX. Subsequently, the mixture was centrifuged and the precipitate was rinsed with ultrapure water until the supernatant changed to colorless. The obtained precipitate was dried and denoted as $CaCO_3$/HA/Glu/DOX. All the supernatants were collected together. To determine the loading efficiency, the amounts of the free DOX in the supernatants were determined by UV–Vis absorbance. The incorporation efficiency is reported using loading content (wt%) and entrapment (wt%) calculated by Equation (1) and (2), respectively. The reported data are the mean values of triplicate determinations ± standard deviation (SD).

$$Loading\ content(\%w/w) = \frac{mass\ of\ DOX\ in\ CaCO_3\ /HA/Glu/DOX \times 100}{mass\ of\ CaCO_3\ /HA/Glu/DOX}$$

(1)

$$Entrapment(\%w/w) = \frac{mass\ of\ DOX\ in\ CaCO_3\ /HA/Glu/DOX \times 100}{mass\ of\ DOX\ used\ in\ formulation}$$

(2)

## 2.5. Evaluation of the in vitro drug release performance

To evaluate the *in vitro* drug release performance of the DOX from CaCO$_3$/HA/Glu/DOX, CaCO$_3$/HA/Glu/DOX (7.0 mg) were dispersed into PBS buffer solutions (7 mL, pH = 5.0, 6.0, 7.4) and shaken at 25 °C. At different predetermined intervals, the suspension was centrifuged and the supernatant (3 mL) was taken out and replaced by fresh PBS solution (3 mL) to continue the drug release evaluation. The DOX concentration in the supernatant was determined by UV–Vis absorbance. The drug release efficiency was calculated by Equation (3). The data were reported as mean ± SD based on triplicate measurements.

$$DOX\ release(\%w/w) = \frac{mass\ of\ DOX\ in\ supernatant \times 100}{mass\ of\ DOX\ used\ in\ formulation} \quad (3)$$

## 2.6. Cell culture

In the present study, V79-4 Chinese hamster lung cells (ATCC No. CCL-93) and HeLa human cervical carcinoma cells (ATCC No. CCL-2) were selected as the model normal and cancer cells, respectively. The cells were cultivated in Eagle's minimum essential medium (EMEM) supplemented with heat-inactivated FBS (10%), Penicillin (100 units/mL), Streptomycin (100 μg/mL), amphotericin B (fungizone, 0.25 μg/mL) and sodium bicarbonate (2.2 μg/mL) in a humidified incubator with 5% CO$_2$ at 37 °C.

## 2.7. Evaluation of cytotoxic effects

HeLa or V79-4 single-cell suspensions (100 μL) with initial cell density of $2.5 \times 10^4$ cells/mL were pre-seeded separately in each well of 96-well flat bottom culture microplates for 24 h. Subsequently, free DOX, CaCO$_3$/HA/Glu, and CaCO$_3$/HA/Glu/DOX suspension in EMEM medium were added into the wells and co-incubated for 72 h. The final concentrations of the samples were 0.0061, 0.0122, 0.0244, 0.0488, 0.0977, 0.1953, 0.3906, and 0.7813 μg/mL, respectively. Incubation of cells with EMEM medium rather than samples was prepared as the control. The cytotoxic effects of the free DOX, CaCO$_3$/HA/Glu and CaCO$_3$/HA/Glu/DOX on V79-4 and HeLa cells were measured by MTT colorimetric assay. Briefly, after 72 h treatment, freshly prepared MTT solution (100 μL, 5 mg/mL in PBS) was added to each well and incubated at 37 °C for 5 h. After carefully discard the supernatant in each well, the dark blue crystals were dissolved completely by 150 μL of DMSO and the absorbance of the solution in each well at 570 nm was quantified by a microplate reader. The cell proliferation activity was expressed by the absorbance while the cytotoxic effects of the free DOX, CaCO$_3$/HA/Glu, and CaCO$_3$/HA/Glu/DOX were calculated by Equation (4). The data were reported as mean ± SD based on triplicate measurements.

$$Percentage\ of\ inhibition(\%) = \left(1 - \frac{O.D._{570nm}\ of\ treatment\ group}{O.D._{570nm}\ of\ control\ group}\right) \times 100$$

$$(4)$$
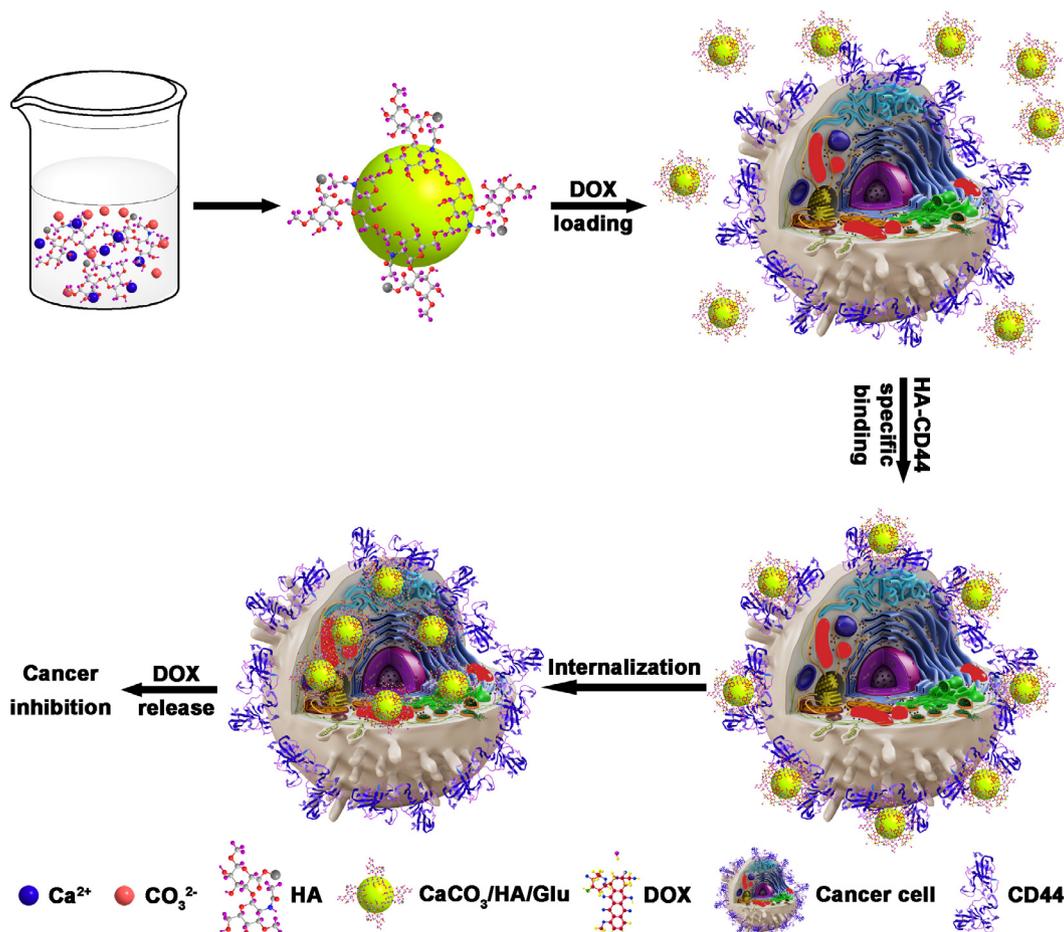


**Scheme 1.** Preparation of CaCO$_3$/HA/Glu MHSs, efficient loading of DOX, targeted delivery, specific internalization, and significant inhibition of cancer cells.

## 2.8. Determination of [Ca²⁺]

To determine [$Ca^{2+}$], CaCO₃/HA/Glu was incubated in EMEM medium or co-incubated with V79-4 or HeLa cells for 72 h. Subsequently, the mixtures were centrifuged to remove any possible solid samples completely. Then the supernatants were diluted with HNO₃ (2%) and analyzed using inductively coupled plasma-mass spectrometer (ICP-MS, ELAN DRC-e, Perkin–Elmer Sciex) to determine [$Ca^{2+}$]. For comparison, [$Ca^{2+}$] in pure EMEM medium was also determined.

## 2.9. Transmission electron microscopy (TEM) of cells

HeLa cells were treated by CaCO₃/HA/Glu/DOX for 12 h. The cells were collected, fixed with glutaraldehyde (2.5%) and washed with PBS. Subsequently, post-fixation with osmium tetroxide (1%) was performed followed by washed with PBS, dehydration with ascending series of alcohol before embedding in Spurr. Ultrathin sections with 70 nm were cut by Leica Reichert ultracut and doubly stained with uranyl acetate and lead citrate. Images were acquired using TEM.



**Fig. 1.** (a) SEM, (b) TEM images and (c) size distribution histogram of CaCO₃/HA/Glu MHSs. Inset: magnified SEM image. (d and e) FE-SEM images of CaCO₃/HA/Glu MHSs. (f) Size distribution histogram of nanoclusters in CaCO₃/HA/Glu MHSs. (g) XRD patterns of different samples. The diffraction peaks of calcite and vaterite are highlighted by solid circle (●) and triangle (▼), respectively.

## 3. Results and discussion

The facile preparation of CaCO₃/HA/Glu MHSs, the efficient loading of DOX, the targeted delivery, and the specific and significant treatment of cancer cells can be illustrated in Scheme 1. Firstly, CaCl₂ aqueous solution was added dropwise into mixed aqueous solution of Glu and HA and moderate stirred for 2 h at 25 °C. Then, Na₂CO₃ aqueous solution was added and reacted for 24 h at 25 °C to prepare MHSs. Secondly, DOX was loaded onto MHSs and targeted delivered to cancer cells through the highly specific interaction of HA with CD44 receptors overexpressed on cancer cells' membrane. Thirdly, CaCO₃/HA/Glu/DOX was specifically internalized by cancer cells through macropinocytosis. Finally, CaCO₃ are gradually decomposed in the acidic microenvironment of cancer cells to release the DOX to treat cancer.

### 3.1. Characterization

In this study, the CaCO₃/HA/Glu MHSs were investigated through SEM and TEM observations. From the results shown in Fig. 1a–c, CaCO₃/HA/Glu MHSs are well-dispersed hollow spheres with the average diameter of 975 nm. Furthermore, SEM image shown in Fig. 1d indicates that the shell thickness of the MHSs is about 50 nm. From Fig. 1e and f, CaCO₃/HA/Glu MHSs are composed of nanoclusters with the average size of 25.88 nm.

The XRD patterns of the products prepared under different conditions are shown in Fig. 1g. The diffraction peaks of calcite and vaterite are denoted as solid circle (●) and solid triangle (▼), respectively. From the results, the product prepared in the sole presence of Glu is calcite, similar to the sample prepared in water. This shows that the presence of Glu does not affect the crystal phase of the product. The products prepared in the sole presence of HA or the co-presence of Glu and HA are both the mixture of calcite and vaterite. Based on these results, except to affect the morphology of the product, the co-presence of Glu and HA can also adjust the crystal phase of the product.

From the control experiment, the product prepared in the absence of HA and Glu is not hollow spheres, but cubic-like aggregates (Fig. S1a). The products prepared in the sole presence of Glu or HA are not hollow spheres yet, but irregular aggregates for Glu or solid spheres for HA (Fig. S1b and c). These results reveal that the simultaneous presence of HA and Glu are critical for the successful formation of CaCO₃/HA/Glu MHSs.

Furthermore, from TG-DSC curves of CaCO₃/HA/Glu MHSs shown in Fig. 2a, the weight of the sample gradually decreases by 4.83% from 100 to 610 °C, accompanied with an exothermic peak at 281 °C. Combined with the results of Glu and HA shown in Fig. 2b and c, it can be concluded that the weight loss of CaCO₃/HA/Glu MHSs can be attributed to the combustion of HA and Glu. This reveals that the presence of HA and Glu in MHSs and the HA and Glu contents in MHSs is 4.83%.

From multipoint BET analysis result shown in Fig. 3a, the specific surface area of CaCO₃/HA/Glu MHSs is determined to be 26.07 m²g⁻¹. Surprisingly, from pore size distribution analysis result shown in Fig. 3b, two different types of pores with the diameters of 3.55 nm and 17.71 nm can be clearly seen, revealing the presence of two types of mesopores in MHSs [31]. This mesoporous structure can provide the potential loading space for anticancer drugs.

### 3.2. DOX loading and the incorporation efficiency

In the present study, the possible application of CaCO₃/HA/Glu MHSs as pH-responsive carrier for anticancer drug was evaluated using DOX as model anticancer drug. From the results shown in
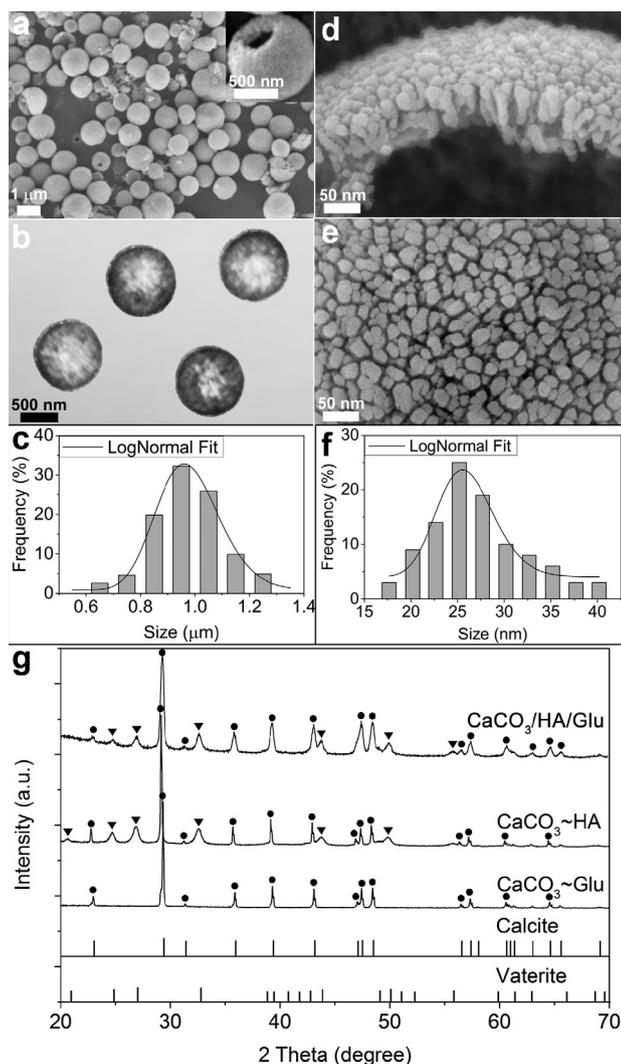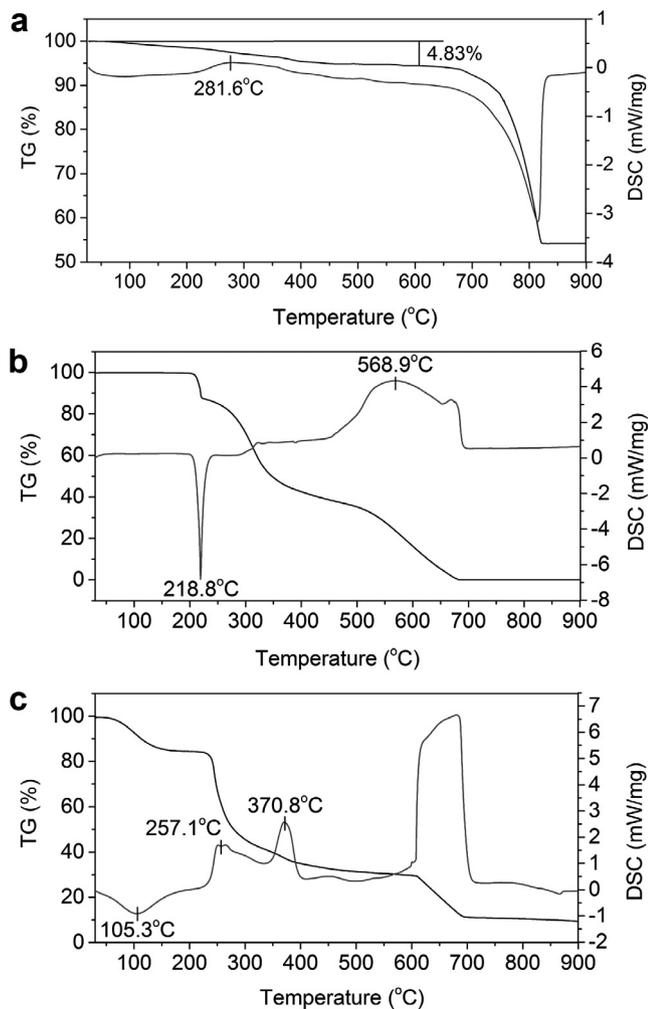
**Fig. 2.** TG-DSC curves of (a) CaCO₃/HA/Glu MHSs, (b) Glu and (c) HA.
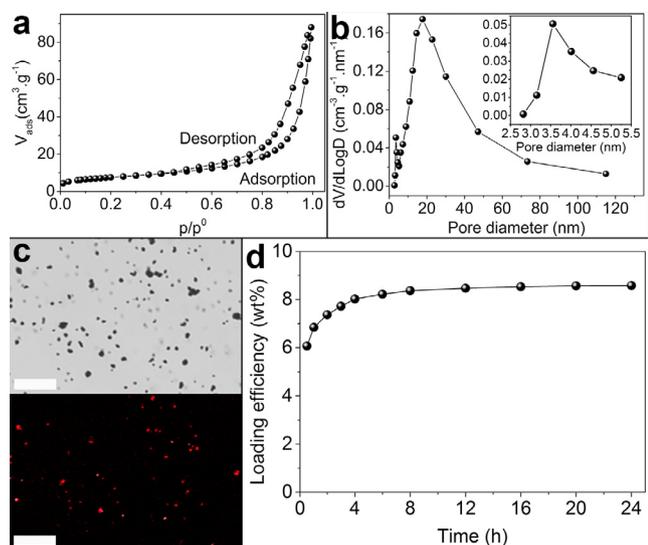


**Fig. 3.** (a) Nitrogen adsorption/desorption isotherm, (b) pore size distribution of CaCO₃/HA/Glu MHSs. (c) Light (up) and fluorescence (down) micrographs of CaCO₃/HA/Glu/DOX. Scale bar: 50 μm. (d) Loading kinetics of DOX into CaCO₃/HA/Glu MHSs.
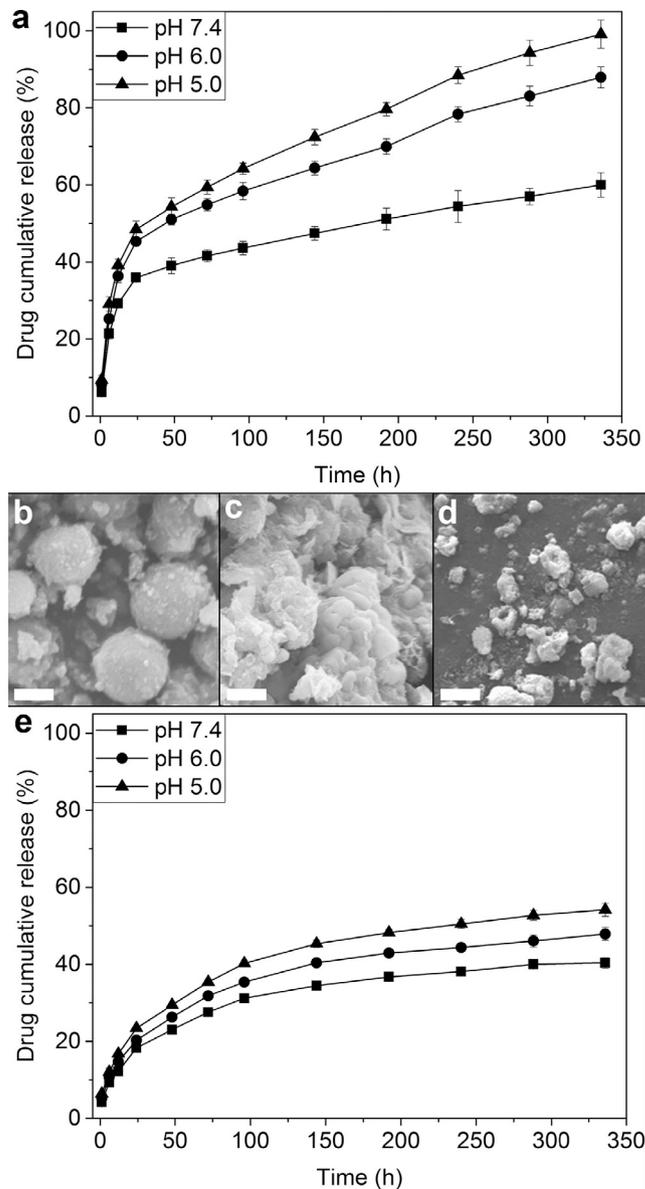


**Fig. 4.** (a) *In vitro* release profiles of CaCO₃/HA/Glu/DOX under different pH. Each data represents the mean ± S.D., n = 3. (b–d) SEM image of CaCO₃/HA/Glu MHSs incubated in release buffers with pH 7.4, 6.0, and 5.0 for 3 d, respectively. Scale bar: 500 nm. (e) *In vitro* release profiles of PS coated CaCO₃/HA/Glu/DOX under different pH. Each data represents the mean ± S.D., n = 3.

Fig. 3c, CaCO₃/HA/Glu/DOX emits strong red color, which can be attributed to the autofluorescence of DOX. This indicates that CaCO₃/HA/Glu MHSs can efficiently load DOX. From the loading kinetic curve shown in Fig. 3d, the loading content (wt%) and entrapment (wt%) can be determined to be 8.587% and 85.87%, respectively. The efficient DOX loading might be ascribed to the presence of mesopores in CaCO₃/HA/Glu MHSs.

## 3.3. In vitro drug release performance

The *in vitro* drug release evaluation result revealed that the as-prepared CaCO₃/HA/Glu MHSs could be used as DDS for pH-responsive and sustained release of DOX. From previous studies, tumor tissues own the more acidic microenvironment than normal

tissues [32]. This is the intrinsic feature of tumor phenotype and generally can be used as the drug-release stimulus for pH-responsive DDS. Therefore, in order to study the pH sensitivity of the drug release from CaCO$_3$/HA/Glu MHSs, the *in vitro* drug release profiles of CaCO$_3$/HA/Glu/DOX were evaluated in buffers with different pH values mimicking tumor and normal tissues. From Fig. 4a, after 14 days of release, the cumulative DOX release is 59.97% for pH 7.4, 87.89% for pH 6.0, and 99.15% for pH 5.0, respectively. It is clearly that the release profiles under acidic conditions are significantly better than that of the neutral physiological condition, which might be attributed to the gradual decomposition of CaCO$_3$/HA/Glu MHSs. This is supported by the SEM observation of the MHSs incubated in buffers with different pH values. From the results shown in Fig. 4b, the spherical morphology of the CaCO$_3$/HA/Glu MHSs is well preserved in neutral buffer. In comparison, CaCO$_3$/HA/Glu MHSs incubated in acidic buffers broke into small pieces (Fig. 4c and d), suggesting the gradual decomposition of CaCO$_3$/HA/Glu MHSs under acidic conditions. To confirm the contribution of decomposition of CaCO$_3$/HA/Glu MHSs under acidic conditions to the release of DOX, CaCO$_3$/HA/Glu/DOX was coated by polystyrene (PS) and the drug release profiles under different pH were determined. From the results (Fig. 4e), after coated by PS, the cumulative DOX release is significantly lower than that from the CaCO$_3$/HA/Glu/DOX at the same time point. Moreover, the differences of the cumulative DOX release between the acidic and neutral conditions of the PS coated CaCO$_3$/HA/Glu/DOX are much lower than those of the CaCO$_3$/HA/Glu/DOX. These confirm the contribution of acidic decomposition of CaCO$_3$/HA/Glu MHSs to the release of DOX. In addition, the increased hydrophilicity and higher solubility of DOX at lower pH also contribute to the

pH-dependent release of DOX. At lower pH, the protonation of -NH$_2$ groups on DOX is increased, which reduce the interaction between DOX and carrier and enhance the release of the DOX [33,34]. These results strongly suggest that the CaCO$_3$/HA/Glu MHSs prepared in the current study might be used as a pH-responsive carrier to release anticancer drugs in response to the acidic microenvironment of tumors. Additionally, DOX release occurs in an obviously sustained manner over the period of 14 days. This can acquire the desired DOX level to exert anticancer activity for much longer duration than the free drug and reduce the administration frequency considerably.

### 3.4. Cytotoxic effects of pure DOX and CaCO$_3$/HA/Glu/DOX

In the current study, the cytotoxic effects of samples on V79-4 normal cells and HeLa cancer cells were evaluated by MTT colorimetric assay and the results are shown in Fig. 5a and b. From the results, in the first place, the IC$_{50}$ value of CaCO$_3$/HA/Glu/DOX for V79-4 cells is determined to be 0.2032 μg/mL after 3 days of treatment, which is significantly higher than that of the free DOX (0.1396 μg/mL) and reveals the significant alleviation of the side effect of DOX after loading onto CaCO$_3$/HA/Glu MHSs. In the second place, the IC$_{50}$ value of CaCO$_3$/HA/Glu/DOX for HeLa cancer cells is determined as 0.0113 μg/mL, which is obviously lower than that of the free DOX (0.0801 μg/mL). This reveals the considerable augmentation of the treatment effect of DOX after loaded onto CaCO$_3$/HA/Glu MHSs.

As a single-chain, single-pass, transmembrane glycoprotein, CD44 is frequently overexpressed in various cancer cells [35]. All forms of CD44 contain an N-terminal, membrane-distal,
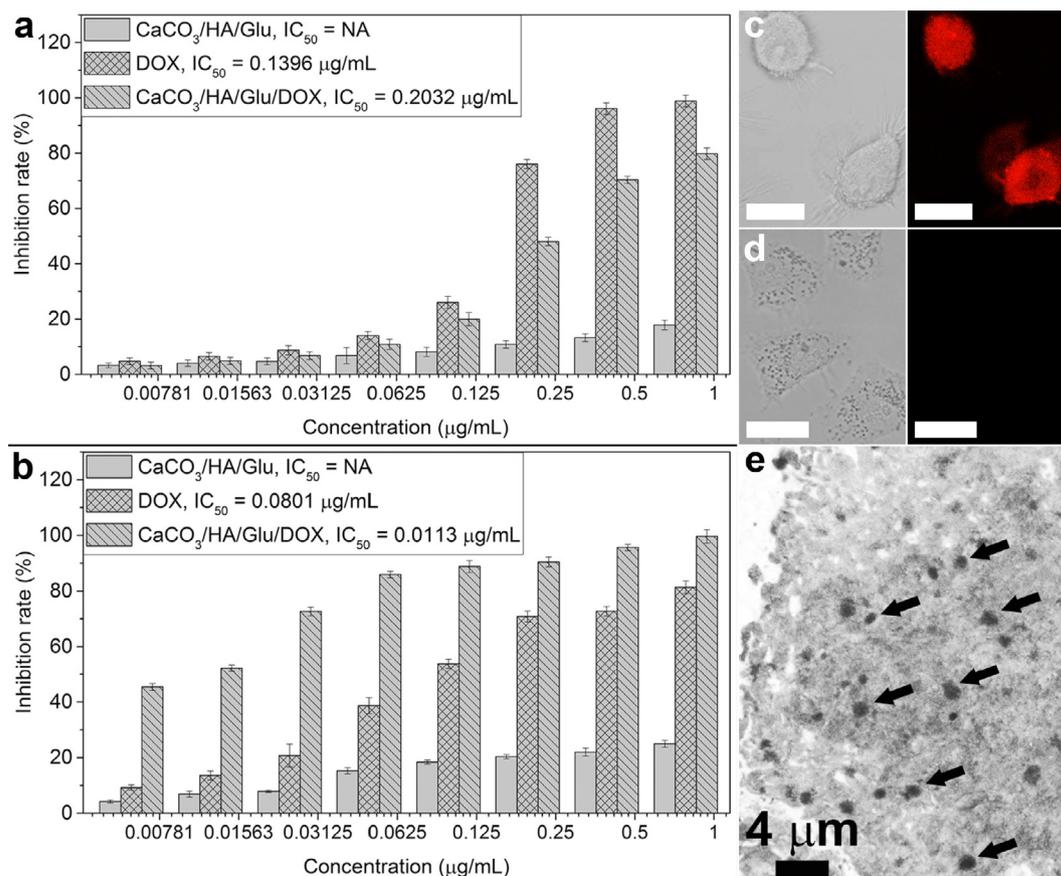


**Fig. 5.** Cytotoxic effects of free DOX, CaCO$_3$/HA/Glu, and CaCO$_3$/HA/Glu/DOX on (a) V79-4 and (b) HeLa cells after 3-d treatment. Each data represents the mean ± S.D., n = 3. Light (left) and fluorescence (right) micrographs of (c) HeLa cells and (d) V79-4 cells after treated with CaCO$_3$/HA/Glu/DOX for 12 h. Scale bar: 20 μm. (e) TEM image of HeLa cell after treated with CaCO$_3$/HA/Glu/DOX for 12 h. The dark arrows highlight the CaCO$_3$/HA/Glu/DOX within the HeLa cell.

hyaluronan-binding domain that has significant homology with the hyaluronan-binding region and can specifically combine with HA [26,36]. From Fig. 5c, after treated by CaCO$_3$/HA/Glu/DOX for 12 h, HeLa cancer cells emit strong red autofluorescence of DOX. However, V79-4 normal cells do not emit the red autofluorescence of DOX (Fig. 5d). This reveals the targeted delivery and macropinocytosis of CaCO$_3$/HA/Glu/DOX into HeLa cancer cells rather than V79-4 normal cells. From TEM image of HeLa cells after treated with CaCO$_3$/HA/Glu/DOX for 12 h (Fig. 5e), it can clearly observe the presence of CaCO$_3$/HA/Glu/DOX within HeLa cells (dark dots indicated by dark arrows). This further demonstrates the macropinocytosis of CaCO$_3$/HA/Glu/DOX by HeLa cells.

From literature, the treatment efficacy of a chemotherapeutic drug can be judged by specificity between normal cells and cancer cells, which generally can be represented by the ratio of IC$_{50}$ value for normal cells to that for cancer cells. The higher ratio hints the better specificity [37]. According to this concept, the specificities of free DOX and CaCO$_3$/HA/Glu/DOX are calculated to be 1.74 and 17.98, respectively. The specificity of the DOX is significantly enhanced by 10.33-fold through loaded onto CaCO$_3$/HA/Glu MHSs, much better than our previous reports [28,29]. This can be ascribed to the specific delivery feature of CaCO$_3$/HA/Glu/DOX to target cancer cells. Through ICP-MS analysis, the intracellular [Ca$^{2+}$] in CaCO$_3$/HA/Glu/DOX treated HeLa cells is determined as 175.3 µg/mL, much higher than those in culture medium (79.7 µg/mL) and V79-4 cells (102.6 µg/mL). This should be ascribed to the targeted delivery and macropinocytosis of CaCO$_3$/HA/Glu/DOX and gradual dissolution and decomposition of CaCO$_3$ in the weak acidic microenvironment of HeLa cells, which results in the sustained release of DOX. The obvious morphological change of the CaCO$_3$/HA/Glu/DOX incubated with HeLa cells rather than with V79-4 cells observed by SEM further demonstrated the gradual dissolution and decomposition of CaCO$_3$ in the weak acidic microenvironment of HeLa cells (Fig. S2).

## 4. Conclusions

In the present study, CaCO$_3$/HA/Glu MHSs are successfully prepared through a facile approach. The characteristics of the CaCO$_3$/HA/Glu MHSs, including the presence of mesopores, the specific ligand-receptor interaction between HA and CD44, and the pH-sensitivity to the weak acidic microenvironment of cancer cells, endow them with the efficient loading, targeted delivery, pH-responsive and sustained release of anticancer drugs to treat human cancers with high specificity. These suggest that inorganic microscaled materials can be used as the important DDS to specifically and significantly treat human cancers.

## Acknowledgements

## Appendix A. Supplementary material

Supplementary data associated with this article can be found, in the online version, at http://dx.doi.org/10.1016/j.jcis.2017.04.085.

## References

[1] E. Jin, B. Zhang, X. Sun, Z. Zhou, X. Ma, Q. Sun, J. Tang, Y. Shen, E. Van Kirk, W.J. Murdoch, Acid-active cell-penetrating peptides for in vivo tumor-targeted drug delivery, J. Am. Chem. Soc. 135 (2013) 933–940.

[2] E.A. Kuczynski, D.J. Sargent, A. Grothey, R.S. Kerbel, Drug rechallenge and treatment beyond progression-implications for drug resistance, Nat. Rev. Clin. Oncol. 10 (2013) 571–587.

[3] E. Brown, M. Markman, Tumor chemosensitivity and chemoresistance assays, Cancer 77 (1996) 1020–1025.

[4] Y. Pommier, O. Sordet, S. Antony, R.L. Hayward, K.W. Kohn, Apoptosis defects and chemotherapy resistance: molecular interaction maps and networks, Oncogene 23 (2004) 2934–2949.

[5] B. Delalat, V.C. Sheppard, S. Rasi Ghaemi, S. Rao, C.A. Prestidge, G. McPhee, M.-L. Rogers, J.F. Donoghue, V. Pillay, T.G. Johns, N. Kroger, N.H. Voelcker, Targeted drug delivery using genetically engineered diatom biosilica, Nat. Commun. 6 (2015) 8791.

[6] S. Mura, J. Nicolas, P. Couvreur, Stimuli-responsive nanocarriers for drug delivery, Nat. Mater. 12 (2013) 991–1003.

[7] T.M. Allen, P.R. Cullis, Drug delivery systems: entering the mainstream, Science 303 (2004) 1818–1822.

[8] R. Langer, New methods of drug delivery, Science 249 (1990) 1527–1533.

[9] M.A. Moses, H. Brem, R. Langer, Advancing the field of drug delivery: taking aim at cancer, Cancer Cell 4 (2003) 337–341.

[10] P. Pamies, A. Stoddart, Materials for drug delivery, Nat. Mater. 12 (2013) 957.

[11] M. Brazil, Controlling the flow, Nat. Rev. Drug Discov. 2 (2003) 510.

[12] E. Kim, D. Kim, H. Jung, J. Lee, S. Paul, N. Selvapalam, Y. Yang, N. Lim, C.G. Park, K. Kim, Facile, template-free synthesis of stimuli-responsive polymer nanocapsules for targeted drug delivery, Angew. Chem. Int. Edit. 49 (2010) 4405–4408.

[13] R. Mo, T. Jiang, R. DiSanto, W. Tai, Z. Gu, ATP-triggered anticancer drug delivery, Nat. Commun. 5 (2014) 3364.

[14] X. Chen, J. Chen, B. Li, X. Yang, R. Zeng, Y. Liu, T. Li, R.J.Y. Ho, J. Shao, PLGA-PEG-PLGA triblock copolymeric micelles as oral drug delivery system: In vitro drug release and in vivo pharmacokinetics assessment, J. Colloid Interf. Sci. 490 (2017) 542–552.

[15] J. Nicolas, S. Mura, D. Brambilla, N. Mackiewicz, P. Couvreur, Design, functionalization strategies and biomedical applications of targeted biodegradable/biocompatible polymer-based nanocarriers for drug delivery, Chem. Soc. Rev. 42 (2013) 1147–1235.

[16] H. Ljusberg-Wahren, F. Seier Nielsen, M. Brogård, E. Troedsson, A. Müllertz, Enzymatic characterization of lipid-based drug delivery systems, Int. J. Pharmaceut. 298 (2005) 328–332.

[17] C.J. Drummond, C. Fong, Surfactant self-assembly objects as novel drug delivery vehicles, Curr. Opin. Colloid In. 4 (1999) 449–456.

[18] F. Muhammad, M. Guo, W. Qi, F. Sun, A. Wang, Y. Guo, G. Zhu, PH-triggered controlled drug release from mesoporous silica nanoparticles via intracelluar dissolution of ZnO nanolids, J. Am. Chem. Soc. 133 (2011) 8778–8781.

[19] X. She, L. Chen, L. Velleman, C. Li, H. Zhu, C. He, T. Wang, S. Shigdar, W. Duan, L. Kong, Fabrication of high specificity hollow mesoporous silica nanoparticles assisted by Eudragit for targeted drug delivery, J. Colloid Interf. Sci. 445 (2015) 151–160.

[20] P. Zhang, F. Cheng, R. Zhou, J. Cao, J. Li, C. Burda, Q. Min, J.-J. Zhu, DNA-hybrid-gated multifunctional mesoporous silica nanocarriers for dual-targeted and microRNA-responsive controlled drug delivery, Angew. Chem. Int. Edit. 53 (2014) 2371–2375.

[21] M. Arruebo, R. Fernández-Pacheco, M.R. Ibarra, J. Santamaría, Magnetic nanoparticles for drug delivery, Nano Today 2 (2007) 22–32.

[22] J.-M. Oh, S.-J. Choi, G.-E. Lee, S.-H. Han, J.-H. Choy, Inorganic drug-delivery nanovehicle conjugated with cancer-cell-specific ligand, Adv. Funct. Mater. 19 (2009) 1617–1624.

[23] Y. Guo, J. Zhang, L. Jiang, X. Shi, L. Yang, Q. Fang, H. Fang, K. Wang, K. Jiang, Facile one-pot preparation of calcite mesoporous carrier for sustained and targeted drug release for cancer cells, Chem. Commun. 48 (2012) 10636–10638.

[24] G. Helmlinger, F. Yuan, M. Dellian, R.K. Jain, Interstitial pH and pO$_2$ gradients in solid tumors in vivo: High-resolution measurements reveal a lack of correlation, Nat. Med. 3 (1997) 177–182.

[25] X. Ma, X. Zhang, L. Yang, G. Wang, K. Jiang, G. Wu, Z. Cui, Z. Wei, Tunable construction of multi-shelled hollow carbonate nanospheres and their potential applications, Nanoscale 8 (2016) 8687–8695.

[26] B.P. Toole, Hyaluronan-CD44 interactions in cancer: Paradoxes and possibilities, Clin. Cancer Res. 15 (2009) 7462–7468.

[27] V.M. Platt, F.C. Szoka, Anticancer therapeutics: Targeting macromolecules and nanocarriers to hyaluronan or CD44, a hyaluronan receptor, Mol. Pharmaceutics 5 (2008) 474–486.

[28] Y. Guo, Q. Fang, H. Li, W. Shi, J. Zhang, J. Feng, W. Jia, L. Yang, Hollow silica nanospheres coated with insoluble calcium salts for pH-responsive sustained release of anticancer drugs, Chem. Commun. 52 (2016) 10652–10655.

[29] Y. Guo, W. Jia, H. Li, W. Shi, J. Zhang, J. Feng, L. Yang, Facile green synthesis of calcium carbonate/folate porous hollow spheres for the targeted pH-responsive release of anticancer drugs, J. Mater. Chem. B 4 (2016) 5650–5653.

[30] X. Ma, H. Chen, L. Yang, K. Wang, Y. Guo, L. Yuan, Construction and potential applications of a functionalized cell with an intracellular mineral scaffold, Angew. Chem. Int. Edit. 50 (2011) 7414–7417.

[31] K.S.W. Sing, D.H. Everett, R.A.W. Haul, L. Moscow, R.A. Pieroffl, J. Rouquerol, T. Siemieni-Ewska, Reporting physisorption data for gas/solid systems with special reference to the determination of surface area and porosity (recommendations 1984), Pure Appl. Chem. 57 (1985) 603–619.

[32] P. Swietach, R.D. Vaughan-Jones, A.L. Harris, A. Hulikova, The chemistry, physiology and pathology of pH in cancer, Phil. Trans. R. Soc. B 369 (2014) 20130099.

[33] J. You, G. Zhang, C. Li, Exceptionally high payload of doxorubicin in hollow gold nanospheres for near-infrared light-triggered drug release, ACS Nano 4 (2010) 1033–1041.

[34] Z. Liu, X. Sun, N. Nakayama-Ratchford, H. Dai, Supramolecular chemistry on water-soluble carbon nanotubes for drug loading and delivery, ACS Nano 1 (2007) 50–56.

[35] D. Naor, S. Nedvetzki, I. Golan, L. Melnik, Y. Faitelson, CD44 in cancer, Crit. Rev. Clin. Lab. Sci. 39 (2002) 527–579.

[36] S. Misra, P. Heldin, V.C. Hascall, N.K. Karamanos, S.S. Skandalis, R.R. Markwald, S. Ghatak, Hyaluronan–CD44 interactions as potential targets for cancer therapy, FEBS J. 278 (2011) 1429–1443.

[37] P. Phatak, F. Dai, M. Butler, M.P. Nandakumar, P.L. Gutierrez, M.J. Edelman, H. Hendriks, A.M. Burger, KML001 cytotoxic activity is associated with its binding to telomeric sequences and telomere erosion in prostate cancer cells, Clin. Cancer Res. 14 (2008) 4593–4602.